

Evolution of flat bands in two-dimensional fused pentagon network

Tomonari Mizoguchi, Mina Maruyama, Yasuhiro Hatsugai, and Susumu Okada
*Department of Physics, University of Tsukuba, Tsukuba, Ibaraki 305-8571, Japan**

(Dated: November 27, 2024)

Theoretical quest of flat-band tight-binding models usually relies on lattice structures on which electrons reside. Typical examples of candidate lattice structures include the Lieb-type lattices and the line graphs. Meanwhile, there can be accidental flat-band systems that belong to neither of such typical classes and deriving flat-band energies and wave functions for such systems is not straightforward. In this work, we investigate the characteristic band structure for the tight-binding model on a network composed of pentagonal rings, which is inspired by the theoretically-predicted carbon-based material. Although the lattice does not belong to conventional classes of flat band models, the exact flat bands appear only for fine-tuned parameters. We analytically derive the exact eigenenergies and eigenstates of the flat bands. By using the analytic form of the Bloch wave function, we construct the corresponding Wannier function and reveal its characteristic real-space profile. We also find that, even away from the exact flat-band limits, the nearly flat band exists near the Fermi level for the half-filled systems, which indicates that the present system will be a suitable platform for questing flat-band-induced correlated electron physics if it is realized in the real material.

I. INTRODUCTION

Flat bands are one of the characteristic dispersion in crystalline systems, where the energy eigenvalue is constant in the entire Brillouin zone. In flat-band systems, the diverging density of states makes the electron-electron correlation prominent. Indeed, exotic correlation-induced phenomena, such as ferromagnetism [1, 2], superconductivity [3–6], Bose-Einstein condensation [7, 8], and the zero-field fractional quantum Hall effect (i.e., the fractional Chern insulators) [9–11], have been pursued in flat-band systems. Recently, from the experimental sides, variety of the flat-band systems have been found or artificially fabricated. Examples include the twisted bilayer graphene [12–15], the kagome metals [16–20], the molecular-based materials [21–23], the cold atoms [24, 25], and the photonic systems [26–29].

From the viewpoint of the fundamental theory, two typical lattice structures for constructing tight-binding Hamiltonians hosting flat bands are known. One is the sublattice-number-imbalanced bipartite (i.e., the Lieb-type) lattices [30, 31], and the other is the line graphs [1] and their variants [32–36]. In both of these two types of lattices, the formation of localized states due to the destructive interference mechanism plays an essential role; such localized states turn to the flat bands in the momentum space representation, and they are dubbed as the compact localized states (CLSs) [37, 38]. Additionally, for these classes of models and their extensions, analytical solutions of the flat-band states can be obtained in a systematic manner [33, 39–42] even though there are multiple flat bands with different energies.

Meanwhile, not all the flat-band models belong to the above two classes, namely, flat bands can appear accidentally. In such cases, in general, there is no systematic method to obtain analytic solutions of the flat bands. Here we consider one of such examples. The lattice structure we study in this paper is depicted in Fig. 1, which is a tight-binding model for the carbon allotrope proposed by two of the authors [43, 44] [45].

The proposed material is of interest in terms of various applications such as H₂ separation [46], the anode for Li ion batteries [47], and desalination [48]. The lattice geometry of Fig. 1 is characteristic in that it consists of a network of fused pentagons. By investigating the evolution of the band structures upon changing the parameters, we find that there are two limiting cases that have exact flat bands. Interestingly, the origin of the flat band in these two cases are quite different, namely, one is due to the destructive interference effect and the other is attributed to the accidental reason. For both of these two limits, we derive the exact flat-band solutions, and elucidate that the flat-band wave functions are completely different to each other. We also find that the nearly flat bands survive even away from the exact flat-band limits, which indicates that the strongly-correlated physics will be feasible in the real materials hosting this network of fused pentagons even though the transfer integrals of the real materials is away from the ideal flat-band limit.

The rest of this paper is structured as follows. In Sec. II, we introduce our tight-binding model, which is inspired by the carbon-network material [43]. Our main results are presented

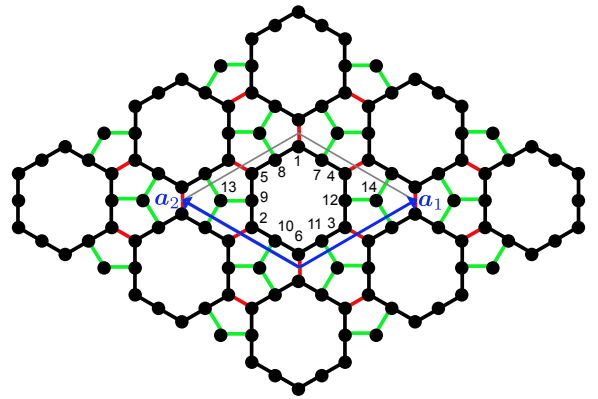


FIG. 1. Lattice structure considered in this paper. Black, red, and green bonds correspond to the transfer integrals t_1 , t_2 , and t_3 , respectively. The lattice vectors are $\mathbf{a}_1 = \left(\frac{\sqrt{3}}{2}, \frac{1}{2}\right)$ and $\mathbf{a}_2 = \left(-\frac{\sqrt{3}}{2}, \frac{1}{2}\right)$.

* mizoguchi@rhodia.ph.tsukuba.ac.jp

in Sec. III, where we show the band-structure evolution upon changing the hopping parameters. The real-space pictures for two exact-flat-band limits are also presented. The summary of this paper is presented in Sec. IV. In Appendix A, we provide a detailed explanation about the flat band for $t_3 = 0$. In Appendix B, we explain the derivation of the analytic solution of the flat bands for $t_1 = t_2 = t_3$. Finally, in Appendix C, we show that we can construct the topological flat band model by introducing the complex next-nearest-neighbor hoppings.

II. MODEL

We consider the tight-binding model defined on a lattice of Fig. 1 for spinless, single-orbital fermions. There are 14 sites per unit cell. In the real space, the Hamiltonian reads $H = \sum_{\langle i,j \rangle} t_{i,j} c_i^\dagger c_j + (\text{h.c.})$, where c_j represents the annihilation operator of the fermion at the site j and $t_{i,j}$ represents the transfer integral between the sites i and j . There are three types of bonds, which we denote by black, red, and green bonds in Fig. 1. Performing the Fourier transform, we obtain the momentum-space representation of the Hamiltonian $H = \sum_{\mathbf{k}} c_{\mathbf{k}}^\dagger \mathcal{H}_{\mathbf{k}} c_{\mathbf{k}}$ where $c_{\mathbf{k}} = (c_{\mathbf{k},1}, \dots, c_{\mathbf{k},14})^T$ and $\mathcal{H}_{\mathbf{k}}$ is the Bloch Hamiltonian in the form of 14×14 matrix:

$$\mathcal{H}_{\mathbf{k}} = \begin{pmatrix} \mathcal{O}_{3,3} & S_{\mathbf{k}} & T_1 & \mathcal{O}_{3,2} \\ S_{\mathbf{k}}^\dagger & \mathcal{O}_{3,3} & T_2 & \mathcal{O}_{3,2} \\ T_1^\dagger & T_2^\dagger & \mathcal{O}_{6,6} & T_{\mathbf{k},3} \\ \mathcal{O}_{2,3} & \mathcal{O}_{2,3} & T_{\mathbf{k},3}^\dagger & \mathcal{O}_{2,2} \end{pmatrix}, \quad (1)$$

where

$$S_{\mathbf{k}} = \begin{pmatrix} 0 & 0 & t_2 e^{i(\theta_{\mathbf{k},1} + \theta_{\mathbf{k},2})} \\ t_2 e^{-i\theta_{\mathbf{k},1}} & 0 & 0 \\ 0 & t_2 e^{-i\theta_{\mathbf{k},2}} & 0 \end{pmatrix}, \quad (2)$$

$$T_1 = \begin{pmatrix} t_1 & t_1 & 0 & 0 & 0 & 0 \\ 0 & 0 & t_1 & t_1 & 0 & 0 \\ 0 & 0 & 0 & 0 & t_1 & t_1 \end{pmatrix}, \quad (3)$$

$$T_2 = \begin{pmatrix} t_1 & 0 & 0 & 0 & 0 & t_1 \\ 0 & t_1 & t_1 & 0 & 0 & 0 \\ 0 & 0 & 0 & t_1 & t_1 & 0 \end{pmatrix}, \quad (4)$$

and

$$T_{\mathbf{k},3} = \begin{pmatrix} t_3 e^{i\theta_{\mathbf{k},1}} & 0 \\ 0 & t_3 e^{i\theta_{\mathbf{k},2}} \\ t_3 & 0 \\ 0 & t_3 e^{-i\theta_{\mathbf{k},1}} \\ t_3 e^{-i\theta_{\mathbf{k},2}} & 0 \\ 0 & t_3 \end{pmatrix}. \quad (5)$$

Here we have used a shorthand notation, $\theta_{\mathbf{k},i} := \mathbf{k} \cdot \mathbf{a}_i$ ($i = 1, 2$). We also note that $\mathcal{O}_{n,m}$ stands for the $n \times m$

zero matrix. The band structure of this model is obtained by solving the eigenvalue problem $\mathcal{H}_{\mathbf{k}} \psi_{\mathbf{k}} = E_{\mathbf{k}} \psi_{\mathbf{k}}$, where $E_{\mathbf{k}}$ is the eigenvalue and $\psi_{\mathbf{k}}$ is the eigenvector in the form of the 14-component column vector. Although we can solve the eigenvalue problem numerically, obtaining the analytic solutions is not easy because the matrix size of $\mathcal{H}_{\mathbf{k}}$ is rather large. Nevertheless, we can obtain the exact solutions of the flat bands for special cases.

III. RESULTS

In this section, we argue the characteristic band structures of the present model. Specifically, we focus on the case where $t_1 = t_2 = -1$ and $t_3/t_1 \in [0, 1]$ is the varying parameter. In Fig. 2, we plot the band structures for several values of t_3/t_1 . We see the exact flat bands in two panels, namely, Fig. 2(a) (i.e., $t_3/t_1 = 0$) and Fig. 2(f) (i.e., $t_3/t_1 = 1$). In the following, we will explain two flat-band limits in detail.

A. Flat-band solutions for two flat band limits

For $t_3/t_1 = 0$ [Fig. 2(a)], the zero energy flat band is three-fold degenerate. In fact, two of these states are trivial, since sublattices 13 and 14 become isolated sites for $t_3 = 0$. The remaining zero-energy flat band can be obtained analytically. A key finding is that T_1 and T_2 of Eqs. (3) and (4) have common kernel, $\mathbf{u} = (1, -1, 1, -1, 1, -1)^T$. Namely, $T_1 \mathbf{u} = T_2 \mathbf{u} = 0$ holds. Having this at hand, we find that the following vector,

$$\psi_{\mathbf{k}} = \frac{1}{\sqrt{6}} (0, 0, 0, 0, 0, 0, 1, -1, 1, -1, 1, -1, 0, 0)^T, \quad (6)$$

satisfies $\mathcal{H}_{\mathbf{k}} \psi_{\mathbf{k}} = 0$ for $t_3 = 0$. This wave function has finite amplitudes on the sites at the edges of the hexagon (sublattices 7-12), and has vanishing amplitudes the sites on the vertices of the hexagon (1-6), which clearly indicates that the flat band arises from the destructive interference effect. It is also worth noting that this zero-energy flat band is robust against changing t_2/t_1 , as far as $t_3 = 0$ is satisfied. Note also that the zero-energy flat band can be understood in terms of the molecular-orbital representation [49–51]. See Appendix A for details.

Next, let us consider $t_3/t_1 = 1$ [Fig. 2(f)]. In this case, we see two exact flat bands, both of which have non-zero eigenenergy. Clearly, these flat bands do not belong to conventional classes arising from the bipartite or line-graph-type lattice structures. Rather, the flat bands in this case realize accidentally, meaning that the clear guiding principle for deriving flat bands is lacking. Nevertheless, we find the exact flat-band solutions in this case, whose derivation is elaborated in Appendix B. We find that, the flat-band energies are given as,

$$E_{\pm} = 1 \pm \sqrt{2}, \quad (7)$$

and corresponding wave functions are

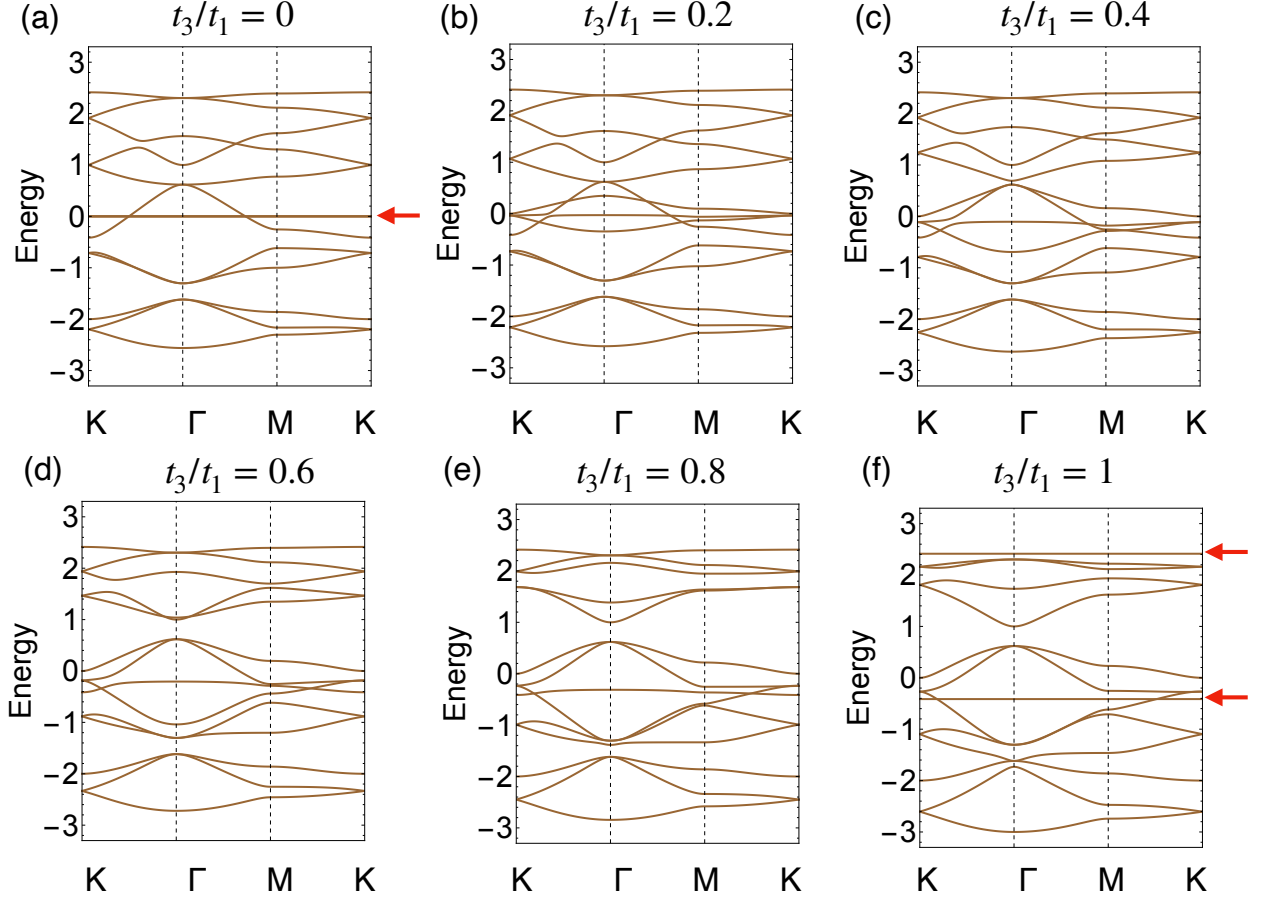


FIG. 2. Band structures of the model of Eq. (1). We fix $t_1 = t_2 = -1$, and vary t_3/t_1 as indicated in each panel. The high-symmetry points in the Brillouin zone are $\Gamma = (0, 0)$, $K = \left(\frac{2\pi}{\sqrt{3}}, \frac{2\pi}{3}\right)$, and $M = \left(\frac{\pi}{\sqrt{3}}, \pi\right)$. Red arrows in the panels (a) and (f) point the exact flat bands.

$$\psi_{\mathbf{k},\pm} = \frac{1}{\mathcal{N}_{\mathbf{k},\pm}} \left(\xi_{\mathbf{k},\pm}, \eta_{\mathbf{k},\pm}, \zeta_{\mathbf{k},\pm}, \eta_{\mathbf{k},\pm}^*, \zeta_{\mathbf{k},\pm}^*, \xi_{\mathbf{k},\pm}^*, 1, 1, 1, 1, 1, 1, -\frac{X_{\mathbf{k}}}{E_{\pm}}, -\frac{X_{\mathbf{k}}^*}{E_{\pm}} \right)^T, \quad (8)$$

where

$$\xi_{\mathbf{k},\pm} = -\frac{2(E_{\pm} - e^{i(\theta_{1,\mathbf{k}} + \theta_{2,\mathbf{k}})})}{E_{\pm}^2 - 1}, \quad (9a)$$

$$\eta_{\mathbf{k},\pm} = -\frac{2(E_{\pm} - e^{-i\theta_{1,\mathbf{k}}})}{E_{\pm}^2 - 1}, \quad (9b)$$

$$\zeta_{\mathbf{k},\pm} = -\frac{2(E_{\pm} - e^{-i\theta_{2,\mathbf{k}}})}{E_{\pm}^2 - 1}, \quad (9c)$$

and

$$X_{\mathbf{k}} = 1 + e^{-i\theta_{\mathbf{k},1}} + e^{i\theta_{\mathbf{k},2}}. \quad (9d)$$

$\mathcal{N}_{\mathbf{k},\pm}$ is the normalization constant. Clearly, these wave functions are completely different from that of Eq. (6). Most remarkably, there is not sublattice that has vanishing amplitude, meaning that the origin of the flat band cannot be attributed to the destructive interference mechanism.

As a by-product of the exact wave functions in Eq. (8), we find that one can construct the topological model with keeping the exact flat bands by introducing the specific form of the imaginary next-nearest-neighbor hoppings. The result is presented in Appendix C.

B. Real-space picture of the exact flat bands

We further address the real-space pictures of the two exact flat-band limits. To this end, we derive the Wannier func-

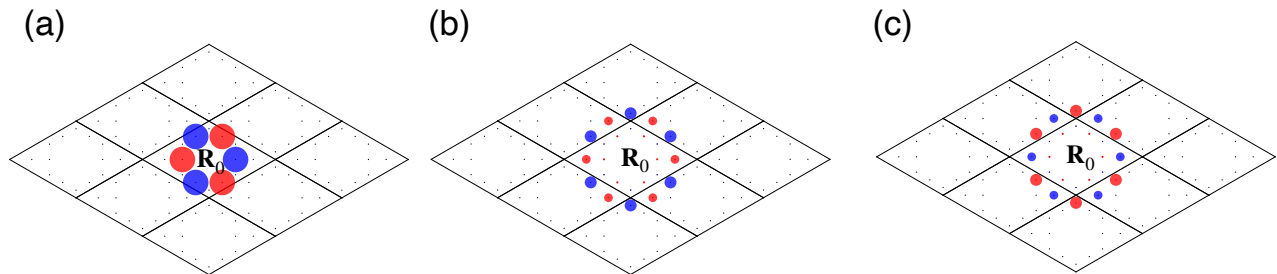


FIG. 3. Real-space distribution of (a) the CLS for $t_3/t_1 = 0$, (b) $w_{\mathbf{R}_0,-}(\mathbf{R}, \alpha)$ for $t_3/t_1 = 1$ and (c) $w_{\mathbf{R}_0,+}(\mathbf{R}, \alpha)$ for $t_3/t_1 = 1$. The red and blue circles indicate that the signs of the wave function are $+$ and $-$, respectively, and the radii of the circles are proportional to $|w|^2$.

tion. In general, computing the Wannier function solely by the numerical diagonalization of the Bloch Hamiltonian requires cautions in the gauge fixing of the wave function at each momentum. In contrast, having the analytical solution at hand, we can straightforwardly calculate the Wannier function. To be concrete, the Wannier function for the flat-band states with centered at the unit cell \mathbf{R}_0 is given as which is localized around the unit cell \mathbf{R}_0 :

$$w_{\mathbf{R}_0}(\mathbf{R}, \alpha) = \frac{1}{N_{\text{u.c.}}} \sum_{\mathbf{k}} e^{i\mathbf{k}\cdot(\mathbf{R}-\mathbf{R}_0)} [\psi_{\mathbf{k}}]_{\alpha}, \quad (10)$$

with $N_{\text{u.c.}}$ being the number of unit cells in the system and α being the sublattice index.

We first consider the $t_3/t_1 = 0$. As we have mentioned, two of the flat bands are obtained by the isolated sites 13 and 14, so we consider the Wannier function corresponding to the Bloch wave function of Eq. (6). As the Bloch wave function of Eq. (6) is \mathbf{k} -independent, \mathbf{k} -summation in Eq. (10) can be taken trivially. We find that the Wannier function is equal to the CLS that has finite amplitudes on finite number of sites and zero amplitude on the remaining sites. This CLS is depicted in Fig. 3(a).

We next consider the case of $t_3/t_1 = 1$. In Figs. 3(b) and 3(c), we depict the real-space profile of the Wannier functions w_{\pm} of several unit cells around the center. We take the summation over \mathbf{k} in Eq. (10) numerically with 72×72 meshes. Note that the Wannier function is real due to the symmetry, $\psi_{-\mathbf{k},\pm} = \psi_{\mathbf{k},\pm}^*$. We see that both of the flat bands have finite amplitudes on all sublattices, which again provides the evidence that simple interference mechanism does not apply to these flat bands. We also see a characteristic real-space profile, namely, the inner small hexagonal plaquette measured from the Wannier center has the small amplitudes whereas the second hexagonal plaquette has the largest amplitudes.

C. Robust nearly flat bands

Tuning to Fig. 2, we find another important feature. Namely, even away from the exact flat band limits [Figs. 2(b)-(e)], there is a reasonably flat band near the Fermi energy of the half-filled case. This indicates that strongly-correlated physics survive even away from the exact flat-band limits. Hence,

the fused pentagon network is a suitable platform for questing flat-band-induced exotic physics.

IV. SUMMARY AND DISCUSSIONS

We have studied the band structure of the tight-binding model of the two-dimensional fused pentagon network. The model is remarkable in that there are two flat-band limits upon changing the hopping parameters. For one limit ($t_3/t_1 = 0$), the flat band is at the zero-energy and its real-space picture is given by the CLS. For another limit ($t_3/t_1 = 1$), the flat bands, appearing in two different energies, realize rather accidentally. The resulting Wannier functions are completely different from the CLS of $t_3/t_1 = 0$. Additionally, upon interpolating these two limits, the bands near the Fermi energy of the half-filled case remain reasonably flat (though it is not exactly flat), which indicates that the strongly-correlated physics due to the nearly-flat bands, such as the emergence of spin-polarized state, is expected throughout the parameter region investigated in this paper.

As for the materials realization, as we have mentioned, the lattice structure is inspired by the prior work on the carbon network [43]. Actually, the band structure obtained by the first-principles calculation is similar to that of the tight-binding model. In the real materials, the fine-tuned conditions for the hopping parameters are not satisfied in general, as the bond length of the black, red and green bonds in Fig. 1 are different among each other. Nevertheless, the fact that the nearly flat band is robust against changing t_3/t_1 indicates that the present carbon network is a suitable candidate for pursuing the flat-band-induced exotic phenomena. Additionally, based on this material, one can make the situation similar to $t_3/t_1 = 0$ by the hydrogen adsorption on the sublattices 13 and 14. Specifically, π -electrons do not live on the adsorbed sites hence the remaining network corresponds to the case of $t_3/t_1 = 0$. Our theoretical results predict that this adsorption changes the nature of the flat band drastically.

Finally, we address the implication of the exact flat bands for $t_3/t_1 = 1$ in the completely different physics, namely, the interacting spin model on the same lattice with the antiferromagnetic coupling. Indeed, in the context of the spin model, the flat band indicates the macroscopically-degenerate magnetic ground state at the classical level [52–57]. In the

present model, we see the exact flat band at on the top for $t_1 = t_2 = t_3 = -1$, meaning that the flat band is on the bottom when reversing the sign of the hoppings, i.e., for $t_1 = t_2 = t_3 = 1$. This indicates the macroscopically-degenerate magnetic ground state for the spin model with the antiferromagnetic coupling, so revealing its ground state will be an interesting future problem.

ACKNOWLEDGMENTS

This work is supported by JSPS KAKENHI Grant No. JP20H05664, JP21K14484, JP21H05232, JP21H05233, JP22H00283, JP23H05469, JP23K03243, and JP23K25788. It is also supported by JST-CREST Grant No. JPMJCR19T1.

Appendix A: Molecular-orbital representation for $t_3 = 0$

In this appendix, we present the insight into the zero-energy flat band for $t_3 = 0$ from the molecular-orbital representation [49–51], by which we clarify the origin of the flat band from the linear-algebraic point of view. The generic framework of the molecular representation is that the zero-energy flat band appears when the $n \times n$ Bloch Hamiltonian $\mathcal{H}_{\mathbf{k}}$ can be represented as

$$\mathcal{H}_{\mathbf{k}} = \Phi_{\mathbf{k}} h_{\mathbf{k}} \Phi_{\mathbf{k}}^\dagger, \quad (\text{A1})$$

where $\Phi_{\mathbf{k}}$ is an $n \times m$ ($m < n$) matrix and $h_{\mathbf{k}}$ is an $m \times m$ Hermitian matrix. Note that $\Phi_{\mathbf{k}}$ can be given by the m sets of the column vector, each of which can be regarded as the (unnormalized) wave function of the molecular orbital:

$$\Phi_{\mathbf{k}} = (\phi_{\mathbf{k},1} \cdots \phi_{\mathbf{k},m}). \quad (\text{A2})$$

The flat band has (at least) $(n-m)$ -fold degeneracy since there exist at least $(n-m)$ vectors $\varphi_{\mathbf{k},\ell}$ satisfying $\Phi_{\mathbf{k}}^\dagger \varphi_{\mathbf{k},\ell} = 0$ due to the fact that $\Phi_{\mathbf{k}}^\dagger$ is the non-square matrix whose number of row is smaller than that of the column.

Let us now consider the case of $t_3 = 0$ of the present model. We omit the sublattices 13 and 14 since they are the isolated sites providing trivial zero-energy flat band. Then the remaining 12×12 block of the Bloch Hamiltonian is given as

$$\mathcal{H}'_{\mathbf{k}} = \begin{pmatrix} \mathcal{O}_{3,3} & S_{\mathbf{k}} & T_1 \\ S_{\mathbf{k}}^\dagger & \mathcal{O}_{3,3} & T_2 \\ T_1^\dagger & T_2^\dagger & \mathcal{O}_{6,6} \end{pmatrix}. \quad (\text{A3})$$

We now show that $\mathcal{H}'_{\mathbf{k}}$ can be expressed in the form of Eq. (A1). To be more specific, we show the explicit form of 11 molecular orbitals by which we can rewrite the Hamiltonian. To this end, we utilize the idea which we have used in Ref. 51. Namely, as a first step, we define 12 molecular orbitals rather than 11, one of which is turned out to be redundant. Specifically, we define

$$\phi_{\mathbf{k},j} = e_j, \quad (\text{A4})$$

for $j = 1, \dots, 6$ and

$$\phi_{\mathbf{k},7} = e_7 + e_8, \quad (\text{A5a})$$

$$\phi_{\mathbf{k},8} = e_8 + e_9, \quad (\text{A5b})$$

$$\phi_{\mathbf{k},9} = e_9 + e_{10}, \quad (\text{A5c})$$

$$\phi_{\mathbf{k},10} = e_{10} + e_{11}, \quad (\text{A5d})$$

$$\phi_{\mathbf{k},11} = e_{11} + e_{12}, \quad (\text{A5e})$$

and

$$\phi_{\mathbf{k},12} = e_{12} + e_7. \quad (\text{A5f})$$

Here, e_j is the unit vector whose j th component is one and all the other components are zero. Defining $\tilde{\Phi}_{\mathbf{k}} = (\phi_{\mathbf{k},1} \cdots \phi_{\mathbf{k},12})$, we can rewrite $\mathcal{H}'_{\mathbf{k}}$ as

$$\mathcal{H}'_{\mathbf{k}} = \tilde{\Phi}_{\mathbf{k}} \tilde{h}_{\mathbf{k}} \tilde{\Phi}_{\mathbf{k}}^\dagger, \quad (\text{A6})$$

where $\tilde{h}_{\mathbf{k}}$ is the 12×12 matrix

$$\tilde{h}_{\mathbf{k}} = \begin{pmatrix} \mathcal{O}_{3,3} & S_{\mathbf{k}} & T'_1 \\ S_{\mathbf{k}}^\dagger & \mathcal{O}_{3,3} & T'_2 \\ T'^{\dagger}_1 & T'^{\dagger}_2 & \mathcal{O}_{6,6} \end{pmatrix}, \quad (\text{A7})$$

with $S_{\mathbf{k}}$ is the same as that of Eq. (2) and

$$T'_1 = \begin{pmatrix} t_1 & 0 & 0 & 0 & 0 & 0 \\ 0 & 0 & t_1 & 0 & 0 & 0 \\ 0 & 0 & 0 & 0 & t_1 & 0 \end{pmatrix}, \quad (\text{A8})$$

$$T'_2 = \begin{pmatrix} 0 & 0 & 0 & 0 & 0 & t_1 \\ 0 & t_1 & 0 & 0 & 0 & 0 \\ 0 & 0 & 0 & t_1 & 0 & 0 \end{pmatrix}. \quad (\text{A9})$$

The key step to obtain the final form of the molecular-orbital representation is to notice that $\phi_{\mathbf{k},7} - \phi_{\mathbf{k},12}$ are not linearly independent with each other [51]. Rather, they satisfy

$$\phi_{\mathbf{k},12} = (\phi_{\mathbf{k},7} + \phi_{\mathbf{k},9} + \phi_{\mathbf{k},11}) - (\phi_{\mathbf{k},8} + \phi_{\mathbf{k},10}). \quad (\text{A10})$$

Using this relation we can rewrite $\mathcal{H}'_{\mathbf{k}}$ in the form of Eq. (A1). Specifically, adopting $\Phi_{\mathbf{k}} = (\phi_{\mathbf{k},1} \cdots \phi_{\mathbf{k},11})$, we set $h_{\mathbf{k}}$ as

$$h_{\mathbf{k}} = \begin{pmatrix} \mathcal{O}_{3,3} & S_{\mathbf{k}} & T''_1 \\ S_{\mathbf{k}}^\dagger & \mathcal{O}_{3,3} & T''_2 \\ T''^{\dagger}_1 & T''^{\dagger}_2 & \mathcal{O}_{5,5} \end{pmatrix}, \quad (\text{A11})$$

where T''_1 and T''_2 are the 3×5 matrices:

$$T''_1 = \begin{pmatrix} t_1 & 0 & 0 & 0 & 0 \\ 0 & 0 & t_1 & 0 & 0 \\ 0 & 0 & 0 & 0 & t_1 \end{pmatrix}, \quad (\text{A12})$$

$$T''_2 = \begin{pmatrix} t_1 & -t_1 & t_1 & -t_1 & t_1 \\ 0 & t_1 & 0 & 0 & 0 \\ 0 & 0 & 0 & t_1 & 0 \end{pmatrix}. \quad (\text{A13})$$

It is again worth mentioning that this molecular-orbital representation holds for any t_1 and t_2 , meaning that the zero-energy flat band exists for any t_1 and t_2 .

Appendix B: Analytic solution of the flat band for $t_1 = t_2 = t_3$

In this appendix, we derive the analytic solution of the flat-band states for $t_1 = t_2 = t_3 = -1$. Unlike the case of $t_3 = 0$, it is not straightforward to find the molecular-orbital representation. Hence, we explicitly solve the Schrödinger equation $\mathcal{H}_k \psi_k = E \psi_k$ where $\psi_k = (\psi_{k,1}, \dots, \psi_{k,14})^T$. Hereafter, we abbreviate the k dependence of $\psi_{k,j}$. A key assumption for obtaining the analytic solution is

$$\psi_7 = \psi_8 = \psi_9 = \psi_{10} = \psi_{11} = \psi_{12}. \quad (\text{B1})$$

We have found this condition by the numerical diagonalization. Without loss of generality, we set $\psi_7 = \psi_8 = \dots = \psi_{12} = 1$; the normalization of the wave function will be considered afterwards.

Under this assumption, we solve the Schrödinger equation explicitly. We first focus on the sublattices 13 and 14, since they are connected only to the sublattices 7-12. By substituting this above assumption into the Schrödinger equation, we have

$$\begin{aligned} -(1 + e^{-i\theta_1} + e^{i\theta_2}) &= E \psi_{13}, \\ -(1 + e^{i\theta_1} + e^{-i\theta_2}) &= E \psi_{14}. \end{aligned} \quad (\text{B2})$$

Then we have $\psi_{13} = -\frac{X}{E}$ and $\psi_{14} = -\frac{X^*}{E}$ [X is defined in Eq. (9d)]. Here we assume $E \neq 0$, which is indeed the case.

We next focus on ψ_1, \dots, ψ_6 , i.e., the vertexes of hexagonal rings. For ψ_1 and ψ_6 , the Schrödinger equation leads to

$$\begin{pmatrix} 0 & -e^{i(\theta_1+\theta_2)} \\ -e^{-i(\theta_1+\theta_2)} & 0 \end{pmatrix} \begin{pmatrix} \psi_1 \\ \psi_6 \end{pmatrix} - \begin{pmatrix} \psi_7 + \psi_8 \\ \psi_{10} + \psi_{11} \end{pmatrix} = E \begin{pmatrix} \psi_1 \\ \psi_6 \end{pmatrix}. \quad (\text{B3})$$

From the assumption $\psi_7 = \dots, \psi_{12} = 1$, we obtain

$$\psi_1 = \psi_6^* = -\frac{2[E - e^{i(\theta_1+\theta_2)}]}{E^2 - 1}. \quad (\text{B4})$$

Note that we additionally assume $E \neq \pm 1$, which is also the case. Similarly, for ψ_2, ψ_3, ψ_4 , and ψ_5 , we obtain

$$\begin{aligned} \psi_2 = \psi_4^* &= -\frac{2(E - e^{-i\theta_1})}{E^2 - 1}, \\ \psi_3 = \psi_5^* &= -\frac{2(E - e^{-i\theta_2})}{E^2 - 1}. \end{aligned} \quad (\text{B5})$$

Lastly, we focus on ψ_7, \dots, ψ_{12} , i.e., the sites on the edges of hexagonal rings. We determine the eigenenergy E so that the assumption of $\psi_7 = \dots = \psi_{12} = 1$ is satisfied self-consistently. For ψ_7 , the Schrödinger equation leads to

$$-(\psi_1 + \psi_4) - e^{i\theta_1} \psi_{13} = E \psi_7. \quad (\text{B6})$$

Substituting Eqs. (B2), (B4), and (B5) into Eq. (B6), as well as $\psi_7 = 1$, we obtain

$$\frac{2}{E^2 - 1}(2E - \alpha) + \frac{1 + \alpha}{E} = E, \quad (\text{B7})$$

where we have defined $\alpha := e^{i(\theta_1+\theta_2)} + e^{i\theta_1}$. Equation (B7) can be rewritten as

$$(E^2 - 2E - 1)(E^2 + 2E - 1 - \alpha) = 0. \quad (\text{B8})$$

As α is actually the k -dependent quantity, the k -dependent solutions of the above equation correspond to Eq. (7) [i.e., $E = 1 \pm \sqrt{2}$]. We note that the conditions for ψ_8, \dots, ψ_{12} lead to the same eigenenergies. Once the eigenenergies are determined, the corresponding wave functions can be obtained from Eqs. (B1), (B2), (B4), (B5), and (B6). The resulting wave functions are shown in Eq. (8).

Appendix C: Topological flat-band model with high Chern numbers

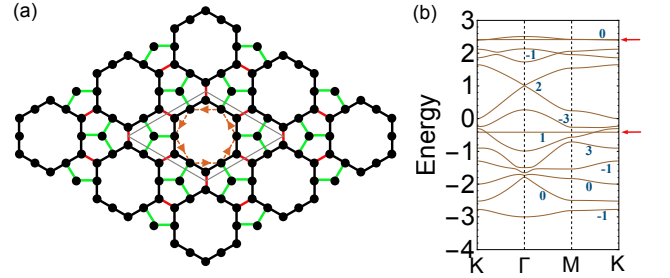


FIG. 4. (a) Schematic figure of additional imaginary hoppings preserving the flat bands. The orange broken lines represent the hopping $-i\lambda$ (in the direction of the arrow). (b) Band structure for $(t_1, t_2, t_3, \lambda) = (-1, -1, -1, 0.3)$. Red arrows point the flat bands.

Here we present the construction of the topological flat-band model based on the present lattice structure, which is inspired by the analytic wave function. In fact, the flat-band wave function of Eq. (8) tells us what kind of additional hopping terms can preserve the exact flat bands. To be concrete, we introduce the pure-imaginary hoppings among the sites 7-12, as shown in Fig. 4(a). This type of imaginary hoppings can be a source of topologically nontrivial states, as proposed in the seminal work by Haldane [58]. The band structure is shown in Fig. 4(b). We also compute the Chern number of each band (or sets of bands if they are degenerate) numerically [59]. We see the exact flat bands are unchanged. This is due to the fact that $\psi_7 = \dots, \psi_{12}$ holds for every k and thus the additional pure-imaginary hoppings vanish when acting on the flat-band wave function. In the present set of parameters, the set of bands containing the flat band E_- has the finite Chern number, whereas that containing E_+ has the vanishing Chern number. We also see that some of the bands has the high Chern number (i.e., the absolute value of the Chern number is larger than 1), which has been of interest recently [60–64].

- [1] A. Mielke, *J. Phys. A: Math. Gen.* **24**, 3311 (1991).
- [2] H. Tasaki, *Phys. Rev. Lett.* **69**, 1608 (1992).
- [3] M. Imada and M. Kohno, *Phys. Rev. Lett.* **84**, 143 (2000).
- [4] S. Peotta and P. Törmä, *Nature Communications* **6**, 8944 (2015).
- [5] H. Aoki, *J. Supercond. Novel Magn.* **33**, 2341 (2020).
- [6] K.-E. Huhtinen, J. Herzog-Arbeitman, A. Chew, B. A. Bernevig, and P. Törmä, *Phys. Rev. B* **106**, 014518 (2022).
- [7] S. D. Huber and E. Altman, *Phys. Rev. B* **82**, 184502 (2010).
- [8] H. Katsura, N. Kawashima, S. Morita, A. Tanaka, and H. Tasaki, *Phys. Rev. Research* **3**, 033190 (2021).
- [9] E. Tang, J.-W. Mei, and X.-G. Wen, *Phys. Rev. Lett.* **106**, 236802 (2011).
- [10] K. Sun, Z. Gu, H. Katsura, and S. Das Sarma, *Phys. Rev. Lett.* **106**, 236803 (2011).
- [11] T. Neupert, L. Santos, C. Chamon, and C. Mudry, *Phys. Rev. Lett.* **106**, 236804 (2011).
- [12] Y. Cao, V. Fatemi, S. Fang, K. Watanabe, T. Taniguchi, E. Kaxiras, and P. Jarillo-Herrero, *Nature* **556**, 43 (2018).
- [13] Y. Cao, V. Fatemi, A. Demir, S. Fang, S. L. Tomarken, J. Y. Luo, J. D. Sanchez-Yamagishi, K. Watanabe, T. Taniguchi, E. Kaxiras, R. C. Ashoori, and P. Jarillo-Herrero, *Nature* **556**, 80 (2018).
- [14] M. Yankowitz, S. Chen, H. Polshyn, Y. Zhang, K. Watanabe, T. Taniguchi, D. Graf, A. F. Young, and C. R. Dean, *Science* **363**, 1059 (2019), <https://www.science.org/doi/pdf/10.1126/science.aav1910>.
- [15] J. M. Park, Y. Cao, K. Watanabe, T. Taniguchi, and P. Jarillo-Herrero, *Nature* **590**, 249 (2021).
- [16] B. R. Ortiz, L. C. Gomes, J. R. Morey, M. Winiarski, M. Bordelon, J. S. Mangum, I. W. H. Oswald, J. A. Rodriguez-Rivera, J. R. Neilson, S. D. Wilson, E. Ertekin, T. M. McQueen, and E. S. Toberer, *Phys. Rev. Mater.* **3**, 094407 (2019).
- [17] J.-X. Yin, S. S. Zhang, G. Chang, Q. Wang, S. S. Tsirkin, Z. Guguchia, B. Lian, H. Zhou, K. Jiang, I. Belopolski, N. Shumiya, D. Multer, M. Litskevich, T. A. Cochran, H. Lin, Z. Wang, T. Neupert, S. Jia, H. Lei, and M. Z. Hasan, *Nature Physics* **15**, 443 (2019).
- [18] M. Kang, S. Fang, L. Ye, H. C. Po, J. Denlinger, C. Jozwiak, A. Bostwick, E. Rotenberg, E. Kaxiras, J. G. Checkelsky, and R. Comin, *Nature Communications* **11**, 4004 (2020).
- [19] Z. Sun, H. Zhou, C. Wang, S. Kumar, D. Geng, S. Yue, X. Han, Y. Haraguchi, K. Shimada, P. Cheng, L. Chen, Y. Shi, K. Wu, S. Meng, and B. Feng, *Nano Letters* **22**, 4596 (2022), pMID: 35536689.
- [20] L. Ye, S. Fang, M. Kang, J. Kaufmann, Y. Lee, C. John, P. M. Neves, S. Y. F. Zhao, J. Denlinger, C. Jozwiak, A. Bostwick, E. Rotenberg, E. Kaxiras, D. C. Bell, O. Janson, R. Comin, and J. G. Checkelsky, *Nature Physics* **20**, 610 (2024).
- [21] A. Kumar, K. Banerjee, A. S. Foster, and P. Liljeroth, *Nano Letters* **18**, 5596 (2018).
- [22] Y. Shuku, R. Suizu, S. Nakano, M. Tsuchiizu, and K. Awaga, *Phys. Rev. B* **107**, 155123 (2023).
- [23] R. Nemoto, R. Arafune, S. Nakano, M. Tsuchiizu, N. Takagi, R. Suizu, T. Uchihashi, and K. Awaga, *ACS Nano* **18**, 19663 (2024).
- [24] S. Taie, H. Ozawa, T. Ichinose, T. Nishio, S. Nakajima, and Y. Takahashi, *Science Advances* **1**, e1500854 (2015).
- [25] H. Ozawa, S. Taie, T. Ichinose, and Y. Takahashi, *Phys. Rev. Lett.* **118**, 175301 (2017).
- [26] S. Xia, A. Ramachandran, S. Xia, D. Li, X. Liu, L. Tang, Y. Hu, D. Song, J. Xu, D. Leykam, S. Flach, and Z. Chen, *Phys. Rev. Lett.* **121**, 263902 (2018).
- [27] D. Leykam and S. Flach, *APL Photonics* **3**, 070901 (2018).
- [28] L. Tang, D. Song, S. Xia, S. Xia, J. Ma, W. Yan, Y. Hu, J. Xu, D. Leykam, and Z. Chen, *Nanophotonics* **9**, 1161 (2020).
- [29] J. Yang, Y. Li, Y. Yang, X. Xie, Z. Zhang, J. Yuan, H. Cai, D.-W. Wang, and F. Gao, *Nature Communications* **15**, 1484 (2024).
- [30] B. Sutherland, *Phys. Rev. B* **34**, 5208 (1986).
- [31] E. H. Lieb, *Phys. Rev. Lett.* **62**, 1201 (1989).
- [32] S. Miyahara, K. Kubo, H. Ono, Y. Shimomura, and N. Furukawa, *Journal of the Physical Society of Japan* **74**, 1918 (2005).
- [33] J. M. Lee, C. Geng, J. W. Park, M. Oshikawa, S.-S. Lee, H. W. Yeom, and G. Y. Cho, *Phys. Rev. Lett.* **124**, 137002 (2020).
- [34] T. Ogata, M. Kawamura, and T. Ozaki, *Phys. Rev. B* **103**, 205119 (2021).
- [35] H. Liu, G. Sethi, S. Meng, and F. Liu, *Phys. Rev. B* **105**, 085128 (2022).
- [36] T. Mizoguchi, Y. Gao, M. Maruyama, Y. Hatsugai, and S. Okada, *Phys. Rev. B* **107**, L121301 (2023).
- [37] M. E. Zhitomirsky and H. Tsunetsugu, *Phys. Rev. B* **70**, 100403 (2004).
- [38] D. L. Bergman, C. Wu, and L. Balents, *Phys. Rev. B* **78**, 125104 (2008).
- [39] T. Mizoguchi, M. Maruyama, S. Okada, and Y. Hatsugai, *Phys. Rev. Materials* **3**, 114201 (2019).
- [40] T. Mizoguchi, H. Katsura, I. Maruyama, and Y. Hatsugai, *Phys. Rev. B* **104**, 035155 (2021).
- [41] D. Heo, J. Lee, A. Zhang, and J.-W. Rhim, *Photonics* **10**, 10.3390/photonics10010029 (2023).
- [42] A. M. Marques, J. Mögerle, G. Pelegrí, S. Flannigan, R. G. Dias, and A. J. Daley, *Phys. Rev. Res.* **5**, 023110 (2023).
- [43] M. Maruyama and S. Okada, *Applied Physics Express* **6**, 095101 (2013).
- [44] M. Maruyama and S. Okada, *Japanese Journal of Applied Physics* **53**, 06JD02 (2014).
- [45] Note that the calculated lattice structure (i.e., the optimal position of the carbon atom) is slightly different from Fig. 1, but the connectivity of the bonds are equivalent.
- [46] L. Zhu, Q. Xue, X. Li, Y. Jin, H. Zheng, T. Wu, and Q. Guo, *ACS Applied Materials & Interfaces* **7**, 28502 (2015).
- [47] T. Zeng, Q. Chen, J. Guo, and H. Wang, *Chemical Physics Letters* **745**, 137225 (2020).
- [48] Y. Niu, K. Meng, T. Xu, J. Wang, X. Xiao, J. Rong, X. Yu, Y. Zhang, and Y. Wei, *Diamond and Related Materials* **140**, 110448 (2023).
- [49] Y. Hatsugai and I. Maruyama, *EPL (Europhysics Letters)* **95**, 20003 (2011).
- [50] T. Mizoguchi and Y. Hatsugai, *EPL (Europhysics Letters)* **127**, 47001 (2019).
- [51] T. Mizoguchi, Y. Kuno, and Y. Hatsugai, *Phys. Rev. B* **104**, 035161 (2021).
- [52] J. M. Luttinger and L. Tisza, *Phys. Rev.* **70**, 954 (1946).
- [53] J. N. Reimers, A. J. Berlinsky, and A.-C. Shi, *Phys. Rev. B* **43**, 865 (1991).
- [54] D. A. Garanin and B. Canals, *Phys. Rev. B* **59**, 443 (1999).
- [55] S. V. Isakov, K. Gregor, R. Moessner, and S. L. Sondhi, *Phys. Rev. Lett.* **93**, 167204 (2004).
- [56] K. Essafi, L. D. C. Jaubert, and M. Udagawa, *Journal of Physics: Condensed Matter* **29**, 315802 (2017).
- [57] T. Mizoguchi, L. D. C. Jaubert, R. Moessner, and M. Udagawa,

- Phys. Rev. B* **98**, 144446 (2018).
- [58] F. D. M. Haldane, *Phys. Rev. Lett.* **61**, 2015 (1988).
- [59] T. Fukui, Y. Hatsugai, and H. Suzuki, *Journal of the Physical Society of Japan* **74**, 1674 (2005).
- [60] F. Wang and Y. Ran, *Phys. Rev. B* **84**, 241103 (2011).
- [61] D. Sticlet, F. Piéchon, J.-N. Fuchs, P. Kalugin, and P. Simon, *Phys. Rev. B* **85**, 165456 (2012).
- [62] S. Yang, Z.-C. Gu, K. Sun, and S. Das Sarma, *Phys. Rev. B* **86**, 241112 (2012).
- [63] Y.-F. Wang, H. Yao, C.-D. Gong, and D. N. Sheng, *Phys. Rev. B* **86**, 201101 (2012).
- [64] M. Trescher and E. J. Bergholtz, *Phys. Rev. B* **86**, 241111 (2012).